

Combination of Single-Voxel Proton MR Spectroscopy and Apparent Diffusion Coefficient Calculation in the Evaluation of Common Brain Tumors

Nail Bulakbasi, Murat Kocaoglu, Fatih Örs, Cem Tayfun, and Taner Üçöz

BACKGROUND AND PURPOSE: MR spectroscopy and apparent diffusion coefficient (ADC) calculation have been used frequently for tumor grading and differentiation during the last decade. We evaluated whether the combination of these two techniques can improve the diagnostic effectiveness of MR imaging in patients with brain tumors.

METHODS: Forty-nine patients with histologically proved brain tumors (eight high- and 12 low-grade astrocytomas, eight metastases, eight nonastrocytic gliomas, seven meningiomas, three dysembryoplastic neuroepithelial tumors (DNETs), and three tuberculomas) were prospectively evaluated with contrast material-enhanced MR imaging, single-voxel proton MR spectroscopy (TE = 135 ms), and diffusion-weighted imaging (b = 0, 500, and 1000 s/mm²) before surgery.

RESULTS: MR spectroscopy could differentiate benign from malignant tumors but was not useful in grading malignant tumors. In the differentiation of malignant from benign tumors, N-acetylaspartate (NAA)/choline (Cho), NAA/Cho + creatine (Cr), lactate/Cr, and alanin/Cr ratios (P < .001) were statistically more significant than NAA/Cr and lactate/lipid ratios (P < .05). Increase in lipid/Cr and alanin/Cr ratios could distinguish metastasis and meningiomas from other tumors, respectively (P < .001). DNETs could be diagnosed by their normal spectra and high ADC values ($116.25 \pm 6.93 \times 10^{-3}$ mm²/s). Increase in lactate/Cr ratio correlated with degree of malignancy (r = -0.71). ADCs were effective for grading malignant tumors (P < .001) but not for distinguishing different tumor types with the same grade. High-grade malignant tumors ($87.16 \pm 10.41 \times 10^{-3}$ mm²/s) had significantly lower ADC values than did low-grade malignant ($115.33 \pm 11.67 \times 10^{-3}$ mm²/s) and benign ($107.69 \pm 8.05 \times 10^{-3}$ mm²/s) tumors. Peritumoral ADCs were significantly higher in low-grade than in high-grade astrocytomas (P < .05).

CONCLUSION: Combination of calculated ADC values from tumoral core and specific relative metabolite ratios acquired by MR spectroscopy added more information to MR imaging in the differentiation and grading of brain tumors and were more useful together than each alone.

Although MR imaging is the most useful radiologic technique in the diagnosis and evaluation of common brain tumors, in some instances it is not effective for differentiation of tumor type or detection of tumor grade. Not only can MR spectroscopy show the abnormal findings in nearly 100% of brain tumors, but also it is useful in the differential diagnosis of brain

tumors and in characterization of metabolic changes associated with tumor progression, degree of malignancy, and response to treatment (1–24).

Diffusion-weighted (DW) imaging and calculation of apparent diffusion coefficients (ADCs) have been used to distinguish the normal white matter areas from necrosis, cyst formation, edema, and solid enhancing tumor (24–33). DW and tensor imaging were very effective in the grading and differentiation of different tumor types (24–44) and in the demarcation of tumors owing to the directional dependence of molecular diffusion (25, 28, 29, 34–38).

In this study, we aimed to evaluate the hypothesis that the combination of MR spectroscopy and ADC calculation could improve the preoperative diagnostic

Received August 6, 2002; accepted after revision September 24.
From the Department of Radiology, Gülhane Military Medical Academy, Ankara, Turkey

Address reprint requests to Nail Bulakbasi, MD, GATA Radiology Department, Etlik 06018 Ankara/TURKEY; e-mail: nbulak@gata.edu.tr

effectiveness of MR imaging in patients with brain tumors, within an acceptable additional acquisition time. The main purposes were as follows: 1) to calculate spectroscopic ratios in the differentiation (benign vs malignant) and grading (low or high) of tumor types, 2) to calculate ADC values in the differentiation (benign vs malignant) and grading (low or high) of tumor types, 3) to evaluate additional findings to distinguish the pathologic subtypes, and 4) to find a correlation, if any, among spectroscopic ratios, ADC values, and pathologic findings.

Methods

Study Population

Forty-nine patients, comprising 32 men and 17 women ranging from 17 to 71 years of age (mean age, 44.6 years), suspected of having a brain tumor were prospectively evaluated with MR imaging, DW imaging, and MR spectroscopy before surgery. Fifteen healthy volunteers were evaluated as a control group that comprised nine men and six women ranging from 20 to 65 years of age (mean age, 40.3 years). All the patients underwent surgical resection or biopsy because of location of their lesions in vital or eloquent anatomic parts of the brain. Informed consent was obtained from all participants for MR examinations and for review of patients' records and images.

MR Imaging Evaluation

All participants were examined by using a 1.5-T superconducting MR imager (Magnetom Vision Plus; Siemens, Erlangen, Germany) with a standard circularly polarized head coil. MR imaging was performed in the same week as the operative procedure. In each participant, axial T1-weighted (650/14 ms [TR/TE]) spin-echo (SE), T2-weighted (2000/80 ms) turbo SE, and fast fluid-attenuated inversion recovery (FLAIR) (9000/2500/110 ms [TR/TE/TI]) images were obtained by using 5-mm section thickness, 210-mm field of view (FOV), and 160 × 256 matrix size. After intravenous administration of gadodiamide 0.2 mg/kg (Omniscan; Amersham Health, Carrigtohill, Ireland), contrast-enhanced T1-weighted SE sequences were obtained in axial, coronal, and sagittal planes.

In all cases, normal, tumoral, and peritumoral regions were defined on the basis of the following imaging features: normal tissue, an area containing no enhancement and normal signal intensity on T2-weighted and DW images; tumoral area, a region containing a well-defined solid portion, contrast enhancement, and abnormal signal intensity on T2-weighted and DW images; peritumoral area, a region containing no enhancement and higher signal intensity on T2-weighted and DW images.

MR Spectroscopic Evaluation

Single-voxel MR spectroscopic data were obtained by using a double-SE point-resolved spectroscopy (PRESS) sequence with one-pulse water signal suppression mainly from metabolically active fleshy parts (contrast-enhanced areas) of the lesions, while avoiding contamination from scalp fat. Anatomically matched sets of spectroscopic data were also obtained in the 15 aged-matched control subjects.

Appropriate automatic shimming and water suppression were achieved by using 4–8-Hz line width, 1-kHz spectral width, and the automated software developed by the manufacturer. Spectroscopic data from cubic volumes of 1.5 × 1.5 × 1.5–2 × 2 × 3 cm were obtained by using the PRESS sequence with 1500/135 ms (TR/TE), 128–256 averages, 1024 data points, and 4000-Hz spectrum width. The acquisition time was

approximately 3.19–6.31 minutes. In most examinations, a voxel size of 2 × 2 × 2 cm³ was employed.

The time domain signal intensity was apodized and processed to remove the residual water signal. Postprocessing of the spectroscopic data consisted of frequency shift and phase and linear baseline corrections after Fourier transformation. In most cases, these processes were automatic, but, where spectra appeared distorted, manual processing was used, particularly for phase and baseline corrections. Frequency domain curve was fitted to Gaussian line shape by using the software provided by the manufacturer to define *N*-acetylaspartate (NAA), choline-containing components (Cho), and creatine and phosphocreatine (Cr) peaks. Metabolic peaks used in the differentiation of the different tumor types were as follows: NAA at 2.02 ppm, Cho at 3.22 ppm, Cr at 3.01 ppm, lipid-containing compounds in the range of 0.9–1.3 ppm. Other metabolic peaks, if any, were also calculated as alanin at 1.5–1.6 ppm and lactate at 1.35 ppm (an inverted β-methyl doublet). The lactate assignment was made on the basis of an inverted doublet due to J coupling of lactate-bound protons at a TE of 135 ms. Metabolite values were calculated automatically from the area under each metabolite peak by using the standard commercial software program provided by the manufacturer. Peak integral values were normalized to the internal Cr peak. Metabolite ratios of NAA/Cho, NAA/Cr, NAA/Cr + Cho, Cho/Cr, lipid/Cr, and, if possible, lactate/Cr, lactate/lipid, and alanin/Cr were calculated.

MR Diffusion Imaging

DW images were obtained by using an axial echo-planar SE sequence (5700/139 ms [TR/TE], one average, 5-mm section thickness, 96 × 128 matrix size, 250 × 250-mm FOV) in 22 seconds. DW images and ADC maps were acquired by using b values of 0, 500, and 1000 s/mm² applied in the x, y, and z directions. Postprocessing of ADC maps was performed by using standard software on a different workstation. Tumoral core and peritumoral high-signal-intensity areas were sampled manually, while preferably avoiding cystic and necrotic areas. Standard mean ADC values were calculated automatically and expressed in 10⁻³ mm²/s.

Histopathologic Classification

During the surgery, total resection or multiple biopsy specimens, which minimally measured 2 × 2 × 2 cm were obtained from each patient. Specimens were fixed in formalin and submitted for routine hematoxylin-eosin staining in addition to immunohistochemistry for glial fibrillary acidic protein.

After the detection of tumor type, presence of necrosis, astrogliosis, and macrophage infiltration were noted for each patient. Tumors were graded by using World Health Organization II criteria. For statistical purposes, all tumors were classified as benign or malignant, and the later were subdivided into low (grade 2) or high (grade 3 or 4) grade, as shown in Table 1.

Statistical Analysis

Three experienced neuroradiologists (N.B., C.T., and T.U.) separately evaluated the MR images, spectroscopic data, DW images, and ADC maps. The mean and standard deviations of all MR spectroscopy ratios and ADC values were calculated. On the basis of their basic evaluation, the neuroradiologists were asked to differentiate the tumors into benign or malignant and then to subcategorize the malignant group into low- or high-grade tumors. As a last step, they tried to make histopathologic diagnosis of tumor type on the basis of all imaging findings. A final decision was achieved by consensus.

Data were analyzed with multivariate repeated-measures analysis of variance among the tumor groups to compare benign versus malignant, low grade versus high grade, and differ-

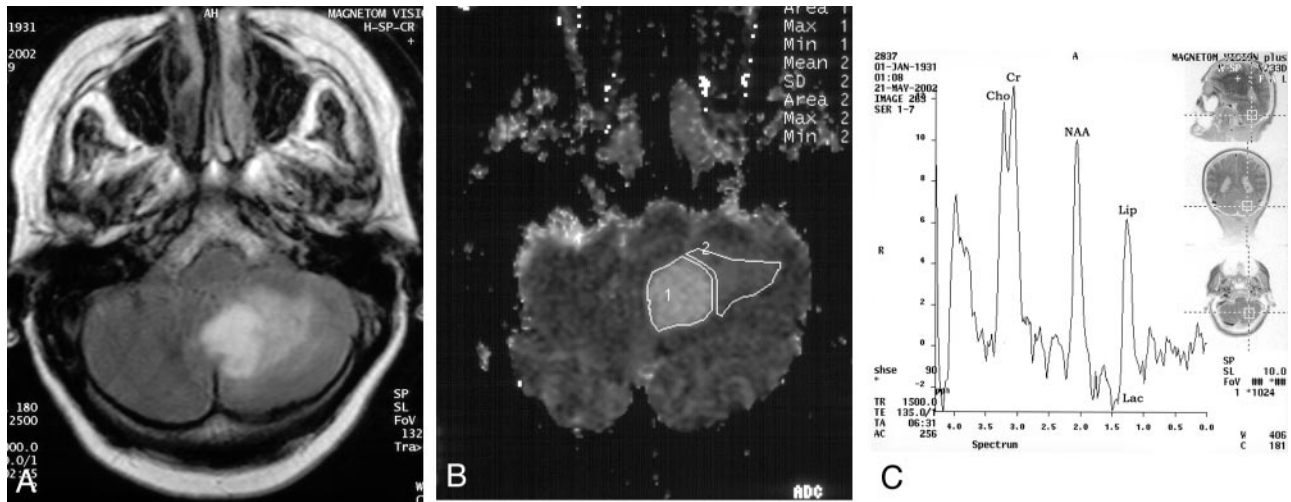


FIG 1. 71-year-old woman with brain metastasis from ovarian cancer.

A, FLAIR image shows a high-signal-intensity necrotic tumor with prominent peritumoral edema. Irregular ringlike enhancement was seen on the T1-weighted image (not shown).

B, ADC map shows the tumor (1) and adjacent edema (2) have higher signal intensity than does the cerebellar parenchyma. Calculated ADC value ($83 \times 10^{-3} \text{ mm}^2/\text{s}$), which is significantly lower than that of low-grade astrocytomas and nonastrocytic gliomas, helps to differentiate metastasis from low-grade malignant tumors, but not from high-grade ones.

C, MR spectrum shows low NAA level (NAA/Cho = 0.92) with prominent lactate and lipid peaks (lipid/Cr = 0.58). High lipid/Cr ratio helps to differentiate metastasis from other primary malignant tumors.

ent tumor types. A nondirectional Tukey post hoc procedure was used where appropriate to correct for the effect of multiple comparisons. The correlation between different parameters was tested by a two-tailed Pearson test. The mean difference was significant at the .05 level. In the comparison of different tumor types, dysembryoplastic neuroepithelial tumors (DNETs, $n = 3$) and tuberculomas ($n = 3$) were excluded from statistical analysis because of insufficient sampling number.

Results

Forty-nine high-quality MR examinations with appropriate histologic diagnosis were available for the evaluation. Thirty-six (74%) of the 49 patients had malignant tumors, and 13 (26%) had benign tumors (Table 1). On the basis of histologic diagnosis, the malignant tumors were subdivided into 16 high-grade (33%) and 20 low-grade (41%) malignant tumors. High-grade astrocytoma included anaplastic astrocytoma and glioblastoma multiforme together. All non-astrocytic tumors were histologically defined as low grade (grade 1 or 2). The benign tumors consisted of seven meningiomas (14%), three tuberculomas (6%), and three DNETs (6%).

MR Spectroscopic Findings

Although there was no major challenge in differentiating benign and malignant tumors from normal brain parenchyma with MR imaging, MR spectroscopy differentiated the benign and malignant tumors from control group in all cases ($P < .001$) (Table 2). The most significant parameter used to differentiate benign tumors from the control group was the alanin/Cr ratio ($P < .001$), and it mainly distinguished the meningiomas from other tumors. NAA/Cho and NAA/Cho + Cr ratios were also useful to differenti-

ate the benign tumors from the control group ($P < .05$). The NAA/Cho, NAA/Cr, NAA/Cho + Cr, lactate/Cr, and lactate/lipid ratios ($P < .001$) were significantly effective in the differentiation of malignant tumors from the control group, followed by Cho/Cr and lipid/Cr ratios ($P < .05$). In the differentiation of malignant tumors from benign ones, the NAA/Cho, NAA/Cho + Cr, lactate/Cr, and alanin/Cr ratios ($P < .001$) were statistically more significant than the NAA/Cr and lactate/lipid ratios ($P < .05$). No significant difference was noted between the Cho/Cr and lipid/Cr ratios in the differentiation of benign versus malignant tumors. Except for the lipid/Cr ratio ($P < .05$), none of the spectroscopic parameters were useful in grading the malignant tumors (Table 3).

The MR spectroscopic parameters of all histologic subtypes are shown in Table 4. Although MR spectroscopic parameters and ADCs of DNETs ($n = 3$) and tuberculomas ($n = 3$) are shown in Table 4, they were excluded from statistical comparison because of their low sampling numbers. Besides the classification as benign versus malignant or low- versus high-grade tumors, the major question was whether MR spectroscopy could distinguish tumor types that were in the same grade, such as high-grade astrocytoma versus metastasis or low-grade astrocytoma versus non-astrocytic low-grade gliomas. No significant difference was noted in NAA/Cho, NAA/Cr, NAA/Cr + Cho, Cho/Cr, lactate/Cr, and lactate/lipid ratios among the different histologic subtypes. The lipid/Cr ratio was significantly effective in distinguishing metastases (Fig 1) from high- (Fig 2) and low-grade astrocytomas (Fig 3), nonastrocytic gliomas (Fig 4) ($P < .001$), and meningiomas (Fig 5) ($P < .05$). Also, the alanin/Cr ratio was useful in distinguishing meningiomas from other tumor types ($P < .001$).

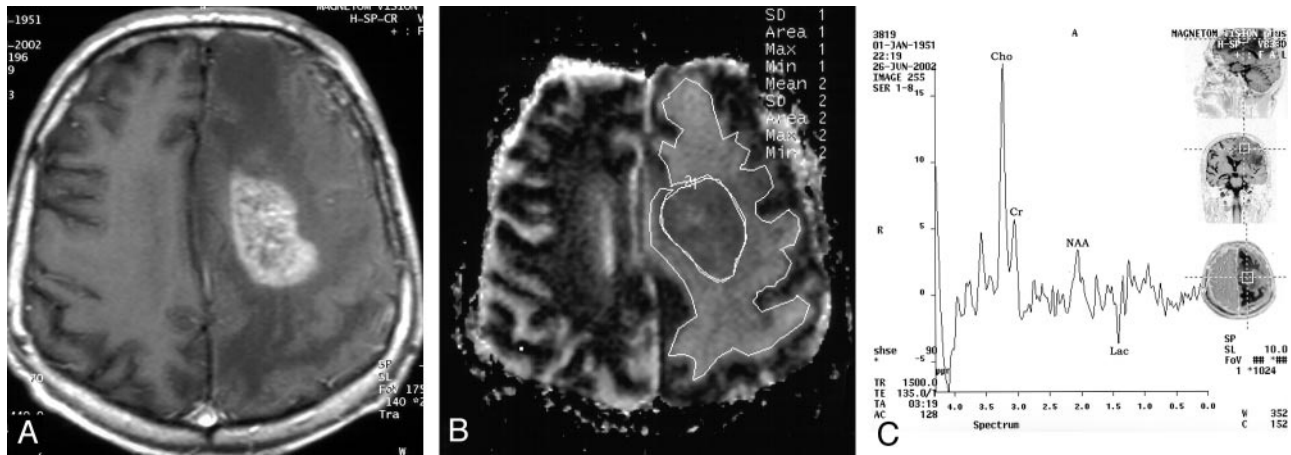


FIG 2. 51-year-old man with high-grade astrocytoma in the left periventricular white matter.
A, T1-weighted image shows heterogeneous contrast enhancement of the tumor with extensive peritumoral edema.
B, ADC map shows that the tumor (1) and adjacent tumor (2) nearly isointense with cerebral white matter (2). This tumor's calculated ADC value is $87 \times 10^{-3} \text{ mm}^2/\text{s}$, which helps to differentiate it from low-grade malignant tumors, but not from metastasis.
C, Proton MR spectrum shows prominent decrease in NAA and increase in Cho (NAA/Cho = 0.19) and lactate (lactate/Cr = 0.28). Absence of prominent lipid peak with low lipid/Cr ratio helps to differentiate this tumor from metastasis.

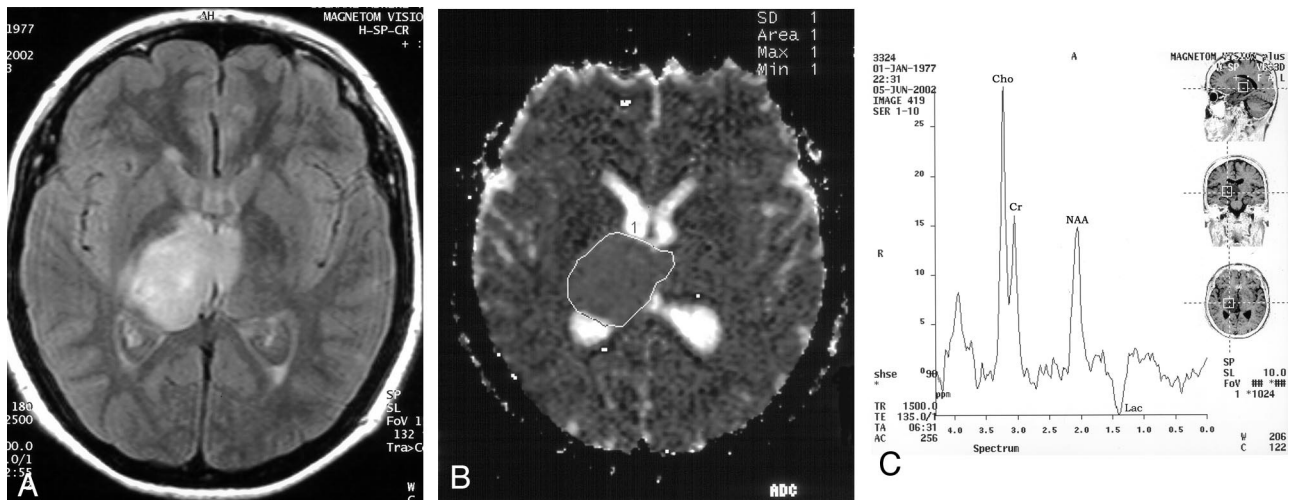


FIG 3. 25-year-old woman with low-grade astrocytoma in right thalamus and subsequent invasion of the left thalamus via the massa intermedia.
A, FLAIR image shows hyperintense tumor without significant edema. Faint enhancement was seen on the T1-weighted image (not shown).
B, ADC map shows that the tumor (1) has slightly higher signal intensity than that of normal thalamus. Calculated ADC value of $110 \times 10^{-3} \text{ mm}^2/\text{s}$ indicates low-grade malignant tumor, but this was not useful to differentiate it from other low-grade malignant tumors.
C, MR spectrum shows decreased NAA/Cho ratio (0.66) with prominent lactate peak. This is a common finding for primary malignant brain tumors, but does not allow us to make a subtype classification.

When compared with control values, the NAA/Cho ratio was decreased in all tumor groups except DNET. No spectroscopic parameter was effective in differentiating DNETs from control group. Although not statistically significant, metastases had relatively higher NAA/Cho ratios than those of other malignant tumors; this was probably due to a relatively much less increase in Cho values than to a decrease in NAA, especially when compared with high-grade astrocytoma. However, a decrease in NAA/Cr ratio was prominent in both benign and malignant tumors, such as high- and low-grade astrocytomas, nonastrocytic gliomas, DNETs, and tuberculomas. This was the result of a prominent decrease in NAA with relative conservation of Cr levels in different tumor groups.

The NAA/Cho + Cr ratio was calculated to evaluate whether or not it made a difference in the diagnosis of brain tumors. All tumor groups had significantly lower NAA/Cho + Cr ratios when compared with control values. The statistical significance of the NAA/Cho + Cr ratio was the same as that of the NAA/Cho ratio.

The Cho/Cr ratios were higher than the control values in all tumors except DNET, which had an insignificantly lower Cho/Cr ratio. The statistical significance of this ratio was always lower than that of all other parameters (in $P < .05$ level), and this ratio did not correlate with any pathologic changes.

Metastases had significantly higher lipid/Cr ratios than those of the other tumors, followed by meningi-

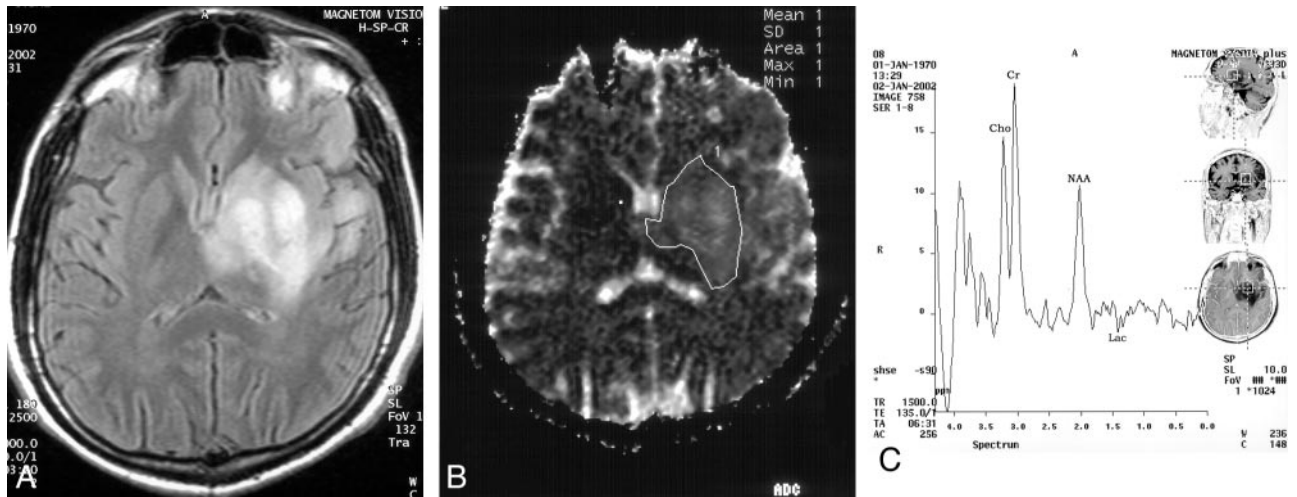


FIG 4. 22-year-old man with oligodendroglioma involving the left temporal lobe and basal ganglia region.

A, FLAIR image shows hyperintense mass without significant edema. No contrast enhancement was present on the T1-weighted image (not shown).

B, ADC map shows that the tumor (t) has a heterogeneous pattern and higher signal intensity than that of the contralateral basal ganglia region. Its calculated ADC value is $118 \times 10^{-3} \text{ mm}^2/\text{s}$ and strongly suggests low-grade malignant or benign tumor.

C, MR spectrum shows mild decrease in both NAA and Cho (NAA/Cho = 0.72) with small lactate peak. This spectrum helps to differentiate this tumor from benign tumors but is not useful to distinguish the histologic subtypes.

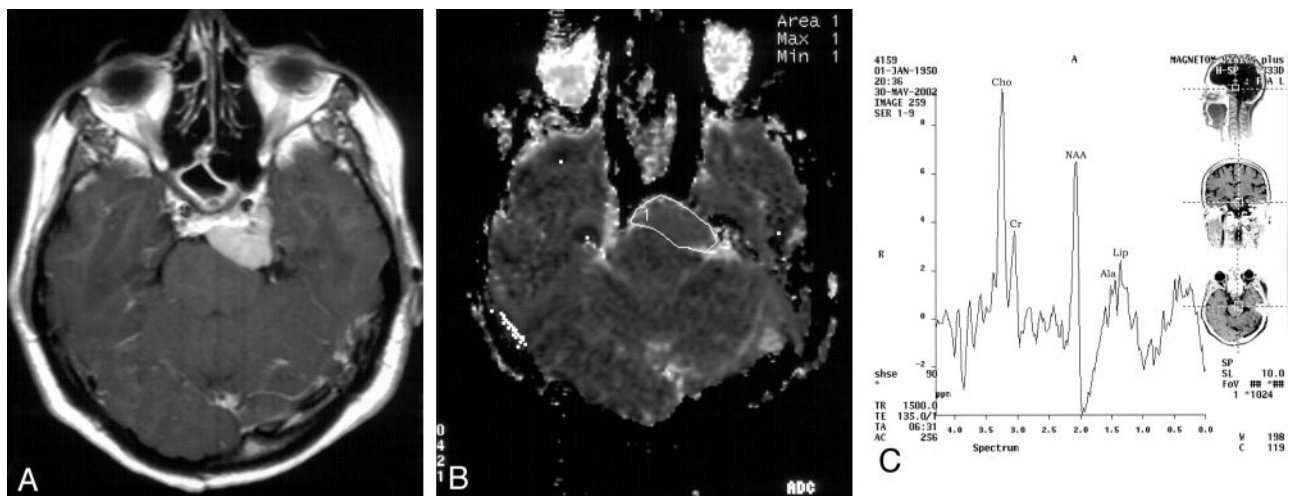


FIG 5. 52-year-old woman with meningioma located in the left prepontine cistern.

A, T1-weighted image shows a well-demarcated, strongly enhanced extraaxial mass.

B, ADC map shows that the tumor (t) has slightly higher signal intensity than that of adjacent brain parenchyma. ADC value of $109 \times 10^{-3} \text{ mm}^2/\text{s}$ does not help to distinguish this tumor from other benign lesions.

C, MR spectrum shows decreased NAA/Cho ratio (0.76) with prominent lipid and alanin peaks at 1.5 ppm (alanin/Cr = 0.68). Prominent alanin peak with low NAA and high Cho levels helps to distinguish meningioma from other tumor groups.

omas, nonastrocytic gliomas, and high-grade astrocytomas in decreasing order. In the other tumor groups, the lipid/Cr ratios were within normal limits except for those of tuberculomas, which were lower than those of the control group. Lactate was detected in all malignant tumors and was more prominent in metastasis and high-grade astrocytomas than nonastrocytic gliomas and low-grade astrocytomas. Increase in the lactate/Cr ratio correlated with an increase in degree of malignancy ($r = -0.71$). The lactate/lipid ratio was useful to differentiate tumor versus normal and benign versus malignant tumors, but was not effective in grading. Alanin was only detected in five (71%) of seven meningiomas, and its level was significantly

high. Alanin could easily distinguish the meningiomas from other tumor types, but was not always present in all meningiomas.

Calculated ADC Values

Calculated ADC values were quite effective for differentiating benign and malignant tumors from normal parenchyma ($P < .001$). They were not useful in the differentiation of tumors as benign versus malignant, but they were significantly effective in grading of malignant tumors ($P < .001$). As shown in Table 2, although ADC values calculated from tumoral areas could not differentiate benign from malignant tu-

mors, peritumoral ADC values were prominently significant ($P < .001$). Because of the lack of peritumoral edema in benign tumors, this was an expected finding and could easily be detected with MR imaging. Although this was a significant finding, ADC calculation had no additional benefit to MR imaging in the differentiation of benign and malignant tumors.

The ADC values calculated from tumoral core ($P < .001$) were significant in the grading of malignant tumors, whereas the ones obtained from peritumoral area ($P > .05$) had no significance (Table 3). High-grade malignant tumors ($87.16 \pm 10.41 \times 10^{-3} \text{ mm}^2/\text{s}$) had significantly lower ADC values than those of low-grade malignant ($115.33 \pm 11.67 \times 10^{-3} \text{ mm}^2/\text{s}$) and benign ($107.69 \pm 8.05 \times 10^{-3} \text{ mm}^2/\text{s}$) tumors. No significant difference was recorded between ADC values of low-grade malignant tumors and those of benign tumors.

As shown in Table 4, although calculated ADC values were useful in grading malignant tumors, they could not be used to distinguish among different tumor types in the same grade. ADC values calculated from primary tumoral areas were lowest in metastases ($84.88 \pm 7.22 \times 10^{-3} \text{ mm}^2/\text{s}$) and high-grade astrocytomas ($89.44 \pm 12.98 \times 10^{-3} \text{ mm}^2/\text{s}$). These were the nearest ADC values to those of normal cerebral white matter. There was no difference between ADCs to distinguish the metastases from high-grade astrocytomas, but ADC values were useful to distinguish high-grade malignant tumors from low-grade astrocytomas ($112.58 \pm 9.44 \times 10^{-3} \text{ mm}^2/\text{s}$, $P < .001$), nonastrocytic gliomas ($119.44 \pm 14.05 \times 10^{-3} \text{ mm}^2/\text{s}$, $P < .001$), and meningiomas ($107.14 \pm 8.03 \times 10^{-3} \text{ mm}^2/\text{s}$, $P < .05$). Although ADC values of meningiomas were a little bit lower than those of low-grade astrocytomas and nonastrocytic gliomas, all these tumors had the same wide range of ADC values, and no statistically significant differences could be detected among them. Granulomas ($100.67 \pm 17.74 \times 10^{-3} \text{ mm}^2/\text{s}$) had the lowest and the DNETs ($116.25 \pm 6.93 \times 10^{-3} \text{ mm}^2/\text{s}$) had the highest ADC values among the benign tumors.

Peritumoral calculated ADC values were significantly higher in low-grade astrocytomas than in high-grade astrocytomas ($P < .05$). No significant peritumoral ADC values were detected in benign tumors except in one patient with an aggressive meningioma.

No correlation was found among spectroscopic ratios, ADC values, and pathologic findings except for a correlation between the Lac/Cr ratio and degree of malignancy ($r = -0.71$).

Tables can be found elsewhere on the journal's website (www.ajnr.org).

Discussion

MR spectroscopy and DW imaging have been used in the evaluation of brain tumors with increasing frequency during the last decade. Lower ADC values were accepted as a marker of higher tumor grades (24–39). Previously reported MR spectroscopic findings in brain tumors included a decrease in NAA, a

marker of neuronal integrity; an increase in Cho involved in increased cell membrane and myelin turnover; and a decrease in Cr, which provides inorganic phosphates for adenosine triphosphate production involved in cellular energetics and osmotic balance (1,2,5–7,11,16–19, 22–24,40–44). Presence of the lactate and lipid peaks were usually consistent with aggressive tumors, reflecting increased anaerobic metabolism and cellular necrosis, respectively (1, 2, 5, 6, 8, 11, 17, 18, 22–24, 40–44). The diagnostic accuracy of MR spectroscopy in differentiating patients from control subjects was 0.96, and in the nonblinded and blinded discrimination of neoplastic from nonneoplastic disease was 0.96 and 0.83, respectively (44), but the use of MR spectroscopy in the differential diagnosis of different tumor types was limited. The additive information of MR spectroscopy led to a 15.4% higher number of correct diagnoses and to 6.2% fewer incorrect and 16% fewer equivocal diagnoses than with MR imaging data alone (23).

One of the major findings in our study was that MR spectroscopy could differentiate benign and malignant tumors from the control group and each other, but was not effective in grading malignant tumors. Decrease in NAA/Cho ratios and presence of lactate peak were the most significant MR spectroscopic parameters in the differentiation of benign from malignant tumors. A decrease in the NAA/Cho ratio is mainly due to both an increase in Cho levels and a decrease in NAA levels (1, 2, 5, 6, 11, 16, 18, 19, 22–24). The NAA level was decreased in both malignant and benign tumors, more prominently in the former, because of the loss of integrity of neurons. In astrocytomas, the NAA level was reduced to 40–70% of its normal value (5, 6, 8, 11, 23). There was a trend of a decrease in NAA level with the advanced tumor grade, as previously reported (23), but we could not find any statistically significant relation between the decrease in NAA level and tumor grade. As stated, the NAA/Cho + Cr ratio was also obtained and its statistical significance determined. No superiority over the NAA/Cho ratio was found. For this reason, additional calculation of the NAA/Cho + Cr ratio was found to be time-consuming. Contrary to previous reports (20), we found the NAA/Cr ratio also useful for differentiating malignant tumors from benign ones, but not for grading the malignancy.

We detected increased Cho levels in all malignant tumors, which was consistent with previous reports (3, 9, 23). The Cho/Cr ratio was the best MR spectroscopic parameter to demonstrate the grade of malignancy (9, 15, 18, 20, 23), but it was not useful for differentiating tumors with the same grade such as high-grade astrocytomas versus metastases or low-grade astrocytomas versus nonastrocytic gliomas. This increase in Cho/Cr ratio was mainly due to increase in Cho levels because of increased membrane turnover and liberation of unbound Cho-containing compounds caused by the destruction of neurons during the malignant process, rather than a decrease in Cr levels, which was quite constant in various metabolic conditions (1, 2, 6, 11). The semiquantitative

Cho value was a reliable predictor of proliferative activity of gliomas (1, 14). Solid tumor components had higher Cho levels than those of necrotic and/or cystic tumor areas (6, 11). Necrotic tumors could also be differentiated from abscesses by their high Cho levels (45).

We did not detect any lactate peak in benign tumors. The lactate/Cr ratio was significantly high in all malignant tumors and correlated well with the degree of malignancy. Although many authors support this correlation between the lactate level and degree of malignancy (6, 11, 9, 23), some report that lactate or lipids were not useful for differential diagnosis (20). We found that the lactate/Cr ratio was not useful in distinguishing malignant tumors with the same grade. Presence of lactate was the indicator of nonfunctioning normal oxidative respiration and increased anaerobic glycolysis (18), and it was represented as a loss of normal brain parenchyma and necrosis on MR images (2).

The lipid/Cr and lactate/lipid ratios were higher in high-grade malignant tumors than in low-grade ones, but this difference was only significant for the lipid/Cr ratio. The lipid/Cr ratio was significantly higher in metastasis than in other primary malignant tumors. As previously reported (5–8, 11, 15, 23), lipid/Cr was the unique spectroscopic parameter to differentiate metastases from high-grade astrocytomas. An increase in lipid levels has been reported as the indicator of necrosis and usually is prominent in nonastrocytic tumors and metastases (5–8, 11, 15, 18, 22, 23). In addition, Castillo and Kwok (8, 11) showed that *myo*inositol was always present in tumors arising in the central nervous system but should be absent in metastases. They found that there was a trend toward a lower *myo*inositol/Cr ratio in higher grade astrocytomas (anaplastic and glioblastoma multiforme), but a higher *myo*inositol/Cr ratio in low-grade astrocytomas compared with that in healthy control subjects (15).

We detected alanin in five of seven meningiomas, and its level was significantly high to differentiate meningiomas from other benign and malignant tumors. Although presence or absence of alanin in meningiomas has been reported in different series (1, 5, 6, 8, 11, 23), the alanin/Cr ratio in meningeal cells was three to four times higher than that found in astrocytes, neurons, and oligodendrocytes (11). It was decreased with the advance of intratumoral necrosis (11). Another reported specific MR spectroscopic finding for meningioma, the absence of neuronal marker NAA (8, 11, 23), was not detected in our study possibly owing to contamination of the voxel with adjacent brain tissue.

Contrary to previous findings (5, 46, 47), tuberculomas were characterized by slightly decreased NAA/Cho and lipid/Cr ratios compared with those of normal cerebral parenchyma. Although lipids are seen in 86% of tuberculomas (47), this controversy is probably due to the small dimensions of tuberculomas compared with the voxel volume. We believed that 2D or 3D chemical shift imaging with relatively small voxel volumes had to be the choice of technique in the

evaluation of such small lesions. In our study, DNETs were easily discriminated from other benign tumors by showing normal spectra, and this finding was consistent with that of a previous report (48).

The second major finding of this study was that calculated ADC values were statistically significant and useful in the grading of malignant tumors. We could not find any significance for the differentiation of the tumors. ADC values obtained from tumor ($P < .001$) and peritumoral area ($P < .05$) were significant in grading tumors but not in differentiating different tumor types in the same grade. As previously reported (36), ADC values helped to distinguish high-grade gliomas from normal tissue but could not be used to separate high-grade gliomas from surrounding edema. ADCs could be used to differentiate normal white matter, edematous brain, and enhancing tumor margins. Anisotropic DW imaging data added no further information to tissue differentiation (37).

Krabbe et al (25) found that ADCs of contrast-enhancing areas and edema surrounding cerebral metastases were significantly higher than those of high-grade astrocytomas. In our study, ADC values calculated from primary tumoral area had the lowest values in high-grade malignant tumors, which had ADC values nearest to those of normal cerebral parenchyma. We could not find any difference among the ADCs of the tumor types in the same grade. Previous findings by Kono et al (32) also support our findings; they demonstrated a good correlation ($r = -0.77$) between ADC and cellularity in gliomas, which is an important histologic determinant of glioma grade, but ADC could not be used in individual cases to differentiate tumor types reliably.

Calculated ADCs from tumoral area were significantly higher in low-grade malignant tumors than in high-grade ones. In different studies, ADC values of different tumors were reported as $150 \times 10^{-7} \text{ cm}^2/\text{s}$ in cerebral astrocytomas (26) and $190\text{--}200 \times 10^{-7} \text{ cm}^2/\text{s}$ in oligodendrogliomas (27). Our values were lower than these because we tried to exclude cystic and necrotic areas, which showed higher ADCs, and mainly sampled from solid portions of the tumors. As previously reported (30–32), the lower ADCs suggested high-grade astrocytomas, whereas higher ADCs suggested low-grade ones. Other histologic features known to influence tumor grade that may also contribute to ADC values included high nuclear cytoplasmic ratio, relatively loose intercellular tumor matrices, and extent of fibrosis and gliosis (24, 31, 32).

The benign tumors had ADC values higher than those of both high-grade malignant tumors and normal cerebral white matter but not higher than those of low-grade malignant tumors. The ADC values of solid gliomas, metastases, and meningiomas were in the same range as previously reported (25, 31). Granulomas had the lowest and DNETs had the highest ADC values among benign tumors, and this was also consistent with the literature (31). Meningiomas, low-grade astrocytomas, and nonastrocytic gliomas had a wide range of similar ADCs. Meningiomas with low ADC values tended to be malignant or highly atypical,

whereas meningiomas with the highest ADC values had increased water content due to either a specific histologic subtype of meningioma or the presence of associated pathologic abnormality (33).

Peritumoral calculated ADC values were significantly higher in low-grade astrocytomas than in high-grade astrocytomas ($P < .05$). This was probably due to insufficient delineation of tumor margins by use of contrast-enhanced areas in the calculation of ADC values. The cause of low peritumoral ADC values in high-grade gliomas most probably was the overlap between peritumoral invasion and edema, which led to decrease in peritumoral ADC values. These areas included a higher amount of malignant tumor cells rather than pure edema, but we did not detect any correlation between peritumoral invasion and calculated ADC values. Contrary to previously reported findings (28), we could not determine the extent or presence of peritumoral neoplastic cell infiltration or differentiate infiltration from peritumoral edema by using ADC maps and ADC calculations (32).

The term "peritumoral" was used to describe the region of abnormal signal intensity surrounding the tumoral core on T2-weighted images, but it was difficult to separate this area especially in nonenhancing tumors. The true peritumoral region was commonly found in normal-appearing brain parenchyma at MR imaging but could be demonstrated with perfusion-weighted imaging or MR spectroscopy (13, 39). Because of using single-voxel MR spectroscopy instead of multivoxel 2D or 3D chemical shift imaging, we did not differentiate tumoral and peritumoral Cho levels; however, elevated Cho levels in the peritumoral region of gliomas but not in metastases have been reported (39). Burtcher et al (13) found pathologic spectra outside the area of contrast enhancement in gliomas and lymphomas but not in nonastrocytic circumscribed tumors such as meningioma, pineocytoma, metastasis, and germinoma. Therefore, we agree with Law et al (39) who decided that the term perienhancing region provided a more reasonable description of the region of abnormal signal intensity surrounding gliomas on T2-weighted images, and that 2D chemical shift imaging is a more reliable technique in the evaluation of this perienhancing region.

Conclusion

Our major findings were as the follows: 1) Malignant brain tumors could easily be differentiated from benign ones by the lower NAA/Cho, NAA/Cho + Cr, NAA/Cr and higher lactate/lipid, lactate/Cr tumor ratios of the former, but not by ADC calculations. 2) Malignant brain tumors could be classified as high or low grade by using the ADC calculations from the tumoral core. No statistically significant MR spectroscopic parameter was detected for the grading of malignant brain tumors. 3) Metastases could be distinguished from high-grade astrocytomas by their high lipid/Cr ratios. 4) Meningiomas could be distinguished from all other tumors by their high alanin/Cr ratios. 5) DNETs could easily be distinguished from

other benign tumors by their normal MR spectra and higher ADC values.

The combination of single-voxel MR spectroscopy and ADC calculation could improve the diagnostic efficacy of MR imaging in the differentiation and grading of brain tumors. MR spectroscopy and DW imaging techniques were insufficient to make a differential diagnosis between the same grade of malignant tumors except for distinguishing metastases from high-grade gliomas. Two-dimensional or 3D chemical shift imaging can provide more detailed spectroscopic information, with the penalty of relatively high examination time.

Acknowledgments

The authors express their gratitude to Tümer Türkbay, MD, for excellent statistical support and to Sadik Ihan and Ercan Çarpik for excellent technical support.

References

1. Bruhn H, Frahm J, Gyngell ML, et al. **Noninvasive differentiation of tumors with use of localized H-1 MR spectroscopy in vivo: initial experience in patients with cerebral tumors.** *Radiology* 1989;172:541-548
2. Segebarth CM, Baleriaux DF, Luyten PR, den Hollander JA. **Detection of metabolic heterogeneity of human intracranial tumors in vivo by H-1 NMR spectroscopic imaging.** *Magn Reson Med* 1990;13:62-76
3. Fulham MJ, Bizzi A, Dietz MJ, et al. **Mapping of brain tumor metabolites with proton MR spectroscopic imaging: clinical relevance.** *Radiology* 1992;185:675-686
4. Baker PB, Glickson JD, Brayn RN. **In vivo magnetic resonance spectroscopy of human brain tumors.** *Top Magn Reson Imaging* 1993;5:32-45
5. Poptani H, Gupta RK, Roy R, Pandey R, Jain VK, Chhabra DK. **Characterization of intracranial mass lesions with in vivo proton MR spectroscopy.** *AJNR Am J Neuroradiol* 1995;16:1593-1603
6. Castillo M, Kwok L, Mukherji SK. **Clinical applications of MR spectroscopy.** *AJNR Am J Neuroradiol* 1996;17:1-15
7. Krouwer HGJ, Kim TA, Rand SD, et al. **Single-voxel proton MR spectroscopy of nonneoplastic brain lesions suggestive of a neoplasm.** *AJNR Am J Neuroradiol* 1998;19:1695-1703
8. Castillo M, Kwok L. **Proton MR spectroscopy of common brain tumors.** *Neuroimaging Clin North Am* 1998;8:733-752
9. Meyerand ME, Pipas JM, Mamourian A, Tosteson TD, Dunn JF. **Classification of biopsy-confirmed brain tumors using single-voxel MR spectroscopy.** *AJNR Am J Neuroradiol* 1999;20:117-123
10. Nelson SJ, Vigneron DB, Dillon WP. **Serial evaluation of patients with brain tumors using volume MRI and 3D 1-H MRSI.** *NMR Biomed* 1999;12:123-128
11. Castillo M, Kwok L. **Clinical applications of proton magnetic resonance spectroscopy in the evaluation of common intracranial tumors.** *Top Magn Reson Imaging* 1999;10:104-113
12. Grand S, Passaro G, Ziegler A, et al. **Necrotic tumor versus brain abscess: importance of amino acids detected at 1-H MR spectroscopy—initial results.** *Radiology* 1999;213:785-793
13. Burtcher IM, Skagerberg G, Geijer B, Englund E, Ståhlberg F, Holtås S. **Proton MR spectroscopy and preoperative diagnostic accuracy: an evaluation of intracranial mass lesions characterized by stereotactic biopsy findings.** *AJNR Am J Neuroradiol* 2000;21:84-93
14. Shimizu H, Kumabe T, Shirane R, Yoshimoto T. **Correlation between choline level measured by proton MR spectroscopy and Ki-67 labeling index in gliomas.** *AJNR Am J Neuroradiol* 2000;21:659-665
15. Castillo M, Smith JK, Kwok L. **Correlation of myo-inositol levels and grading of cerebral astrocytomas.** *AJNR Am J Neuroradiol* 2000;21:1645-1649
16. Bendszus M, Warmuth-Metz M, Klein R, et al. **MR spectroscopy in gliomatosis cerebri.** *AJNR Am J Neuroradiol* 2000;21:375-380

17. Butzen J, Prost R, Chetty V, et al. **Discrimination between neoplastic and nonneoplastic brain lesions by use of proton MR spectroscopy: the limits of accuracy with logical regression model.** *AJNR Am J Neuroradiol* 2000;21:1213-1219
18. Kimura T, Sako K, Gotoh T, Tanaka K, Tanaka T. **In vivo single-voxel proton MR spectroscopy in brain lesions with ring-like enhancement.** *NMR Biomed* 2001;14:339-349
19. Dowling C, Bollen AW, Noworolski SM, et al. **Preoperative proton MR spectroscopic imaging of brain tumors: correlation with histopathologic analysis of resection specimens.** *AJNR Am J Neuroradiol* 2001;22:604-612
20. Schlemmer HP, Bachert P, Herfarth KK, Zuna I, Debus J, van Kaick G. **Proton MR spectroscopic evaluation of suspicious brain lesions after stereotactic radiotherapy.** *AJNR Am J Neuroradiol* 2001;22:1316-1324
21. Tzika AA, Cheng LL, Goumnerova L, et al. **Biochemical characterization of pediatric brain tumors by using in vivo and ex vivo magnetic resonance spectroscopy.** *J Neurosurg* 2002;96:1023-1031
22. Tzika AA, Zarifi MK, Goumnerova L, et al. **Neuroimaging in pediatric brain tumors: Gd-DTPA-enhanced, hemodynamic, and diffusion MR imaging compared with MR spectroscopic imaging.** *AJNR Am J Neuroradiol* 2002;23:322-333
23. Moller-Hartmann W, Herminghaus S, Krings T, et al. **Clinical application of proton magnetic resonance spectroscopy in the diagnosis of intracranial mass lesions.** *Neuroradiology* 2002;44:371-381
24. Sener RN. **Longstanding tectal tumors: proton MR spectroscopy and diffusion MRI findings.** *Comput Med Imaging Graph* 2002;26:25-31
25. Krabbe K, Gideon P, Wang P, Hansen U, Thomsen C, Madsen F. **MR diffusion imaging of human intracranial tumors.** *Neuroradiology* 1977;39:483-489
26. Le Bihan D, Breton E, Lallemand D, Grenier P, Cabanis E, Laval-Jeantet M. **MR imaging of intravoxel incoherent motions: application to diffusion and perfusion in neurologic disorders.** *Radiology* 1986;161:401-407
27. Hajnal JV, Doran M, Hall AS, et al. **MR imaging of anisotropically restricted diffusion of water in the nervous system: technical, anatomic, and pathologic considerations.** *J Comput Assist Tomogr* 1991;15:1-18
28. Tien RD, Felsberg GJ, Friedman H, Brown M, MacFall J. **MR imaging of high-grade cerebral gliomas: value of diffusion-weighted echoplanar pulse sequences.** *AJR Am J Roentgenol* 1994;162:671-677
29. Brunberg JA, Chenevert TL, McKeever PE, et al. **In vivo MR determination of water diffusion coefficients and diffusion anisotropy: correlation with structural alteration in gliomas of the cerebral hemispheres.** *AJNR Am J Neuroradiol* 1995;16:361-371
30. Noguchi K, Watanabe N, Nagayoshi T, et al. **Role of diffusion-weighted echo-planar MRI in distinguishing between brain abscess and tumour: a preliminary report.** *Neuroradiology* 1999;41:171-174
31. Stadnik TW, Chaskis C, Michotte A, et al. **Diffusion-weighted MR imaging of intracerebral masses: comparison with conventional MR imaging and histologic findings.** *AJNR Am J Neuroradiol* 2001;22:969-976
32. Kono K, Inoue Y, Nakayama K, et al. **The role of diffusion-weighted imaging in patients with brain tumors.** *AJNR Am J Neuroradiol* 2001;22:1081-1088
33. Filippi CG, Edgar MA, Uluğ AM, Prowda JC, Heier LA, Zimmerman RD. **Appearance of meningiomas on diffusion-weighted images: Correlating diffusion constants with histopathologic findings.** *AJNR Am J Neuroradiol* 2001;22:65-72
34. Le Bihan D, Douek P, Argyropoulou M, Turner R, Patronas N, Fulham M. **Diffusion and perfusion magnetic resonance imaging in brain tumors.** *Top Magn Reson Imaging* 1993;5:25-31
35. Eis M, Els T, Hoehn-Berlage M, Hossman KA. **Quantitative diffusion MR imaging of cerebral tumor and edema.** *Acta Neurochir Suppl (Wien)* 1994;60:344-346
36. Castillo M, Smith JK, Kwock L, Wilber K. **Apparent diffusion coefficients in the evaluation of high-grade cerebral gliomas.** *AJNR Am J Neuroradiol* 2001;22:60-64
37. Maier SE, Bogner P, Bajzik G, et al. **Normal brain and brain tumor: multicomponent apparent diffusion coefficient line scan imaging.** *Radiology* 2001;219:842-849
38. Sinha S, Bastin ME, Whittle IR, Wardlaw JM. **Diffusion tensor MR imaging of high-grade cerebral gliomas.** *AJNR Am J Neuroradiol* 2002;23:520-527
39. Law M, Cha S, Knopp EA, Johnson G, Arnett J, Litt AW. **High-grade gliomas and solitary metastases: differentiation by using perfusion and proton spectroscopic MR imaging.** *Radiology* 2002;222:715-721
40. Sijens PE, Knopp MV, Brunetti A, et al. **H-1 spectroscopy in patients with metastatic brain tumors: a multicenter study.** *Magn Reson Med* 1995;33:818-826
41. Negendank WG, Sauter R, Brown TR, et al. **Proton magnetic resonance spectroscopy in patients with glial tumors: a multicenter study.** *J Neurosurg* 1996;84:449-458
42. Pruel MC. **Accurate noninvasive diagnosis of human brain tumors by using proton magnetic resonance spectroscopy.** *Nature Med* 1996;2:323-325
43. Tedeschi G, Lundbom N, Raman R, et al. **Increased choline signal coinciding with malignant degeneration of cerebral gliomas: a serial proton magnetic resonance spectroscopy imaging study.** *J Neurosurg* 1997;87:516-524
44. Rand SD, Prost R, Haughton V, et al. **Accuracy of single-voxel proton MR spectroscopy in distinguishing neoplastic from nonneoplastic brain lesions.** *AJNR Am J Neuroradiol* 1997;18:1695-1704
45. Remy C, Grand S, Lai ES, et al. **1H MRS of human brain abscesses in vivo and in vitro.** *Magn Reson Med* 1995;34:508-514
46. Gupta RK, Vatsal DK, Husain N, et al. **Differentiation of tuberculous from pyogenic brain abscesses with in vivo proton MR spectroscopy and magnetization transfer MR imaging.** *AJNR Am J Neuroradiol* 2001;22:1503-1509
47. Jayasundar R, Singh VP, Raghunathan P, Jain K, Banerji AK. **Inflammatory granulomas: evaluation with proton MRS.** *NMR Biomed* 1999;12:139-144
48. Lee DY, Chung CK, Hwang YS, et al. **Dysembryoplastic neuroepithelial tumor: radiological findings (including PET, SPECT, and MRS) and surgical strategy.** *J Neurooncol* 2000;47:167-174